CFD Application to SST Propulsion System

Y.ooba and H.Kodama (Ishikawajima-Harima Heavy Industries)

O.Nozaki, K.Kikutchi, T.Nishizawa and Y.Matsuo (National Aerospace Laboratory)

Abstract

The SST propulsion system will operate in the range from takeoff to high Mach number. The high speed flight causes very high inlet air temperatures and pressures and the high inlet air temperatures and recovery pressures inside the engine make cooling for elements of the engine mandatory to keep the best available construction materials operating satisfactorily. Technology for satisfied cooling requires to understand the heat transfer in the engine, however there are many difficulties to understand detailed phenomena occurred in the engine from limited measurement.

This paper describes some CFD applications for a SST propulsion system which were carried to understand the mechanisms of flowfields and heat transfer in the engine.

Introduction

In Japan, the Hypersonic Transport Propulsion System (HYPR) Project started in 1989 to develop technologies for the propulsion system of a Mach 5 Hypersonic Transport airplane, which could be environmentally acceptable and economically viable. The engine studied is a combined-cycle engine composed of a turbo-jet engine which can operate from taking-off to Mach 3 and a ram-jet engine which can operate beyond Mach 2.5 up to Mach 5. The variable cycle engine concept is applied to the turbo engine to satisfy the conflicting requirements of low noise level at take-off and of high specific thrust at high altitude and flight speed.

In this project, a new design and analysis approach using CFD was demanded for the development of engine components. CFD was found to be extremely helpful and important to explain measured data of the tests conducted in the engine development.

This paper describes the four examples of the CFD applications which were carried out in the HYPR project; three-dimensional unsteady flow analyses of a single stage high pressure turbine including hot streaks from combustion cambers, axisymmetric steady flow analyses of disc cavities of a high pressure compressor, three-dimensional flow analyses of a rim rear cavity with exit guide vanes and three-dimensional steady flow analyses of a turbine disc cavity of a high pressure turbine.

Unsteady Stage Analysis of HP Turbine

Turbines in SST propulsion system operate near the limits of metal temperature capabilities. Temperature nonuniformity at the inlet to the turbine and their migration and redistribution through the turbine are believed to be a major cause of localized overheating of rotor airfoils and passage endwalls, resulting in reduced component life. The physics governing the temperature redistribution process is not well understood and the inability to predict accurately the local gas temperatures in the rotor passage results in overly conservative cooling designs in order to meet turbine life goals. Difficulties in experimental measurements due to the unsteady interactions between stator and rotor prevent to understand the detailed mechanism of hot streaks. In the current study, three-dimensional unsteady stage analysis was conducted to investigate the detailed flow structure through a single stage high pressure turbine with temperature nonuniformity due to hot streaks from a combustor (see Fig.1).

Outline of Numerical method

The governing equations are the time-dependent three-dimensional Reynolds-averaged Navier-Stokes equations. An implicit finite difference scheme which is capable of using large CFD numbers is used. The convection terms are discretized using the TVD scheme developed by Chakravarthy and Osher (1985) and central differencing is used for the diffusion terms. For the implicit time integration approach, a Newton sub-iteration is performed at each time step to increase stability and reduce linearization errors. The number of sub-iterations is 4 for the present study. The turbulence viscosity is determined using Baldwin-Lomax model.

The algorithm in the present code is parallelized for NWT (Numerical Wind Tunnel) which is a parallel supercomputer developed by NAL. Each sub-domain is executed on a different processing element of NWT and exchanges boundary information with neighboring sub-domains in the same and different blade row. Further details on numerical scheme and the algorithm can be found in Matsuo (1991) and Nozaki (1999).

The single stage HP turbine is composed of 28 stator vanes and 57 rotor blades and subjected to hot streaks corresponding to 16 fuel injectors of the combustor. For the present calculation, the number of rotor was decreased to 56 in order to allow a one-hot streak / seven-stator airfoils / fourteen rotor airfoils combination to be simulated with negligible effect on the pitch-to-chord ratio.

Results and Discussions

Figure 2-(a) , 2-(b) and 2-(c) show the time-averaged total temperature contours in the absolute frame of reference at the stator inlet, at the stator trailing edge and downstream of the rotor respectively. The straight lines from hub to casing represent the stator leading edge. The location of midspan are represented by a circular dotted line. At the stator trailing edge, the hot streak hit on the pressure surface of the stator is transported downwards from the midspan due to secondary flow in the stator, while other hot streaks stay at the midspan and the overall shape of the distortions are approximately the same as those of the stator inlet. It is seen that the peak values of the hot streaks are reduced through the stator passage probably due to diffusive mixing. On the other hand, the redistribution of total temperature distribution due to unsteady

This document is provided by JAXA.

effects is observed downstream of the rotor, although the cores of circular distortions are still recognized. The distortion level is significantly attenuated through the rotor.

Internal Flow in HP Compressor Disc Cavities

Due to high Mach number operations, the HP compressor discharge temperature (CDT) reaches 854K at Mach 2.5 Climb. Therefore knowledge of the heat transfer to the HP compressor disc is essential for accurate prediction of the disc stresses and thus the life of the disc.

A schematic diagram of HP compressor multiple disc arrangement of the SST engine is shown in figure 4. Coolant enters the annulus between a rotating shaft and the HP compressor drum in the upstream discs and leaves through the annulus between a rotating shaft and the last disc hub. The flow structure in the multiple rotating cavities formed by the multiple discs of the HP compressor with a rotating shaft running through the bores is considerably complex. However the detailed information on the flow structure is needed for accurate prediction of convective heat transfer in rotating disc cavities.

An axisymmetric Navier-Stokes code was applied to simulate the flow in the multiple rotating cavities, and the calculation results were used in the thermal modelling to predict the disc temperature. The calculated temperatures were compared with measured data obtained in the core engine test.

Outline of Numerical Method

A three-dimensional incompressible RANS code was used as an axisymmetric code. By assuming an incompressible flow, the buoyancy effect was ignored in the calculation. The turbulent viscosity is determined using the two-equation k-ε eddy viscosity turbulence model. Wall functions are used for the turbulence quantities on a solid wall.

The inflow to the annulus between a rotating shaft and the HP compressor drum in the upstream discs was given radially inward in the same way as the engine. The mass flow was obtained from one-dimensional network analyses of secondary air system using the engine test data.

In the core engine test, the HP compressor disc and the rotating shaft were connected, so the rotation speeds of those components were same.

Results and Discussions

Figure 5 shows the calculated velocity vectors in the multiple rotating cavities. Inside the cavities except near disc bores, axial and radial component of the velocities are very small.

The temperature field within the HP compressor disc was obtained through solution of heat conduction equation with finite element solver. The convective boundary conditions were specified by using the results of flow simulation in the multiple rotating cavities. The resultant temperature distribution is shown in figure 6.

Figure 7 shows the comparison between calculated and measured temperatures. The temperatures are normalized by the HP drum metal temperature measured near the coolant air injection hole (TO). A good agreement indicates that the flow structure in the multiple rotating cavities was reasonably captured by the numerical simulation.

Overheating in the LP-turbine Rim Cavity

As for the research and development of the turbo-jet engine, the experimental engine was developed and the ground performance verification was conducted. Subsequently, the high altitude performance testing facility (ATF) was used for the running of the turbo-jet engine under a high altitude / high speed environment.

In the first ATF test, air temperature in LP-turbine rim cavity (see Fig. 8) increased beyond expectations at the Mach 2.5 climb condition. The cause of overheating was not clearly understood from the limited number of measurements.

Thus a numerical simulation was conducted to understand the flow physics behind overheating in the LP turbine rim cavity occurred in the engine test.

Outline of numerical method

A three-dimensional RANS code using unstructured grid was applied to the analyses. Full details of the numerical method are given by Ohkita et al.(1997).

The turbulent viscosity and the turbulent conductivity are determined using the two-equation k-ε eddy viscosity turbulence model. The current code adopts wall functions (Launder and Spalding, 1974). The wall heat transfer is also expressed using the wall functions recommended by Kays and Crawford (1980).

As the rim cavity in question was thought to be the flowfield where secondary cooling air and mainstream strongly interact, a computational grid modeling both regions was used.

The cavity inflow boundary was located at the exit of upstream labyrinth seal. The mass flow and the temperature were obtained from one-dimensional network analyses of secondary air system.

The mainstream inflow boundary was located at the trailing edge of upstream bucket. The profiles of total pressure, total temperature and flow angles obtained from data analysis using an axisymmetric throughflow calculation of LP turbine based on the engine test data, turbulent kinetic energy and dissipation rate were imposed at the boundary.

The static pressure at the outlet boundary was given such that the calculated inlet Mach number matched the data analysis result.

Considering eight EGVs located at circumferentially regular intervals, the calculation region was confined to one-eighth sector including a EGV, and periodic conditions were imposed at the circumferential boundaries.

Results and Discussions

The calculated velocity vectors in the meridional plane at the circumferential location of the EGV leading edge (Pos.1), the pressure side plane (Pos.2) and the suction side plane (Pos.3) are shown in figure 9-(a), 9-(b), 9-(c), respectively. The colors of the arrows represent the level of temperature. These calculated results indicates that the overheating occurred in the engine test was attributed to circumferentially local hot gas ingestion.

Discoloration on rear stator disk surface at cavity as sketched in Figure 11 was observed when the engine was overhauled after the test. This discoloration resulted at locations subjected to high temperature flow during the engine test. The calculated contours of

This document is provided by JAXA.

temperature at the same disk surface is compared in figure 12. The discoloration in the test and the high temperature region in the calculation generally agree in their locations. This suggests that the numerical simulation captures the overall flow structure in the cavity. Both results show that the highest temperature in the cavity may be observed at the circumferential location near the EGV leading edge.

The calculated contours of static pressure on the hub endwall in the mainstream is shown in figure 10. The figure shows that the potential pressure disturbance due to the thickness and turning of the EGV exists over the cavity entry region. This is thought to be the reason why pressure asymmetry was appeared in the cavity and hot gas ingestion was caused.

Internal Flow in HP Turbine Disc Cavity

Flows inside a turbine disc cavity tend to be very complex because of its complicated geometries (see Fig.13). Heat transfer to the turbine disc is strongly influenced by the flow structure in the cavity. Therefore it is essential to know the flowfield inside the cavity for accurate prediction of the heat transfer.

Outline of Numerical Method

In this study, a three-dimensional RANS code was applied to simulate the flows in the turbine disc cavity. Navier-Stokes equations are discretized using a finite volume method in the relative coordinate of the turbine disc. The study is focused on the effect of bolts in the cavity on the flowfield and resultant heat transfer. 30 bolts are located on the rotating wall surface of the turbine disc. One thirtieth domain of the annulus is calculated using the periodic boundary conditions at the circumferential ends. Computational domains both with bolt and without bolt are shown in figure14. Non-slip boundary condition are imposed on the surfaces for both stationary and rotating parts. Inlet and outlet secondary cooling air conditions are set at the inlet boundary of the upper side and the lower side of the cavity using data from the network calculation of the secondary air system.

Results and Discussions

Figure 15, 16 and 17 respectively show velocity vectors, distributions of temperature and swirl ratio inside the turbine disc cavity for the cases both with bolts and without bolts respectively. Swirl ratio is defined as swirl velocity of fluid divided by swirl velocity of the rotating surface at the same radial position. These figures show that flows inside the cavity are strongly influenced by existence of bolts inside the cavity.

Figure 18 compares radial distribution of heat transfer coefficient on the rotor disc. It can be seen that the averaged heat transfer coefficient for the case with bolts well agrees with the experimental results for the configuration with bolts, and the average heat transfer coefficient for the case without bolts would increase by 30%.

Conclusions

Four sets of CFD simulations focused on the prediction of flow and heat transfer applied to the engine of HYPR project were presented. It was found that CFD takes an important role in understanding the phenomena occurred in the SST propulsion system.

References

[1]Chakravarthy, S. R. and Osher, S., "A New Class of High Accuracy TVD Schemes for Hyperbolic Conservation Laws", AIAA 85-0363, 1985.

[2]Baldwin, B. S. and Lomax, H., "Thin-Layer Approximation and Algebraic Model for Separated Turbulent Flows", AIAA 78-257, 1978.

[3]Matsuo,Y., "Computations of Three-Dimensional Viscous Flows in Turbomachinery Cascades", AIAA 91-2237, 1991.

[4]Nozaki, O. et al, "Unsteady Three-Dimensional Viscous Flow Computations of Multiple Blade-Row Interactions", ISABE 99-7032, 1999.

[5]Yamawaki, S. et al, "CFD Contribution to Development of HYPR Engine", AIAA 99-0886, 1999.

[6]Ohkita, Y. et al, "Numerical Simulation of Flow and Heat Transfer in 3D Complicated Geometries Using Unstructured Grids", AIAA 97-1948, 1997.

[7]Launder, B. E. and Spalding, D. B., "The Numerical Computation of Turbulent Flows", Computer Methods in Applied Mechanics and Engineering, Vol.3, pp.269-289, 1974.

[8]Kays, W. M. and Crawford, M. E., "Convective Heat and Mass Transfer", McGraw-Hill, New York.

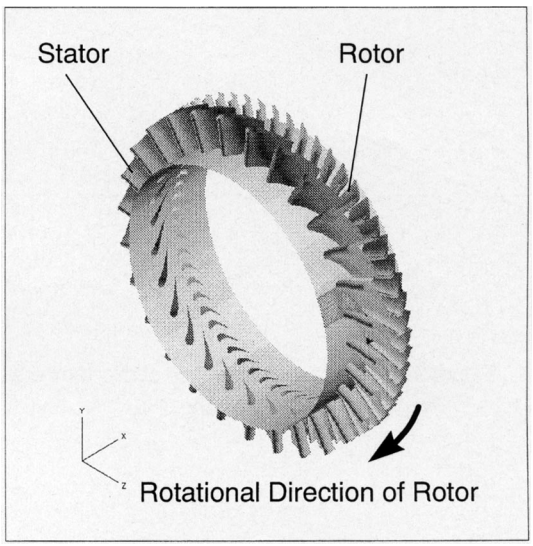

Figure 1 Schematic of single stage high pressure turbine

This document is provided by JAXA.

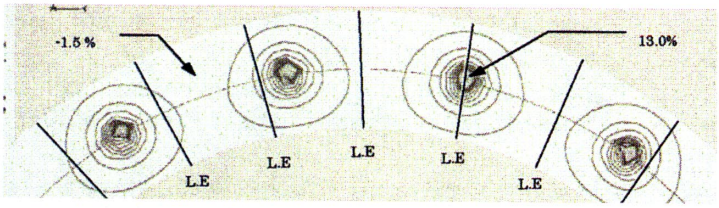

(a) upstream of stators

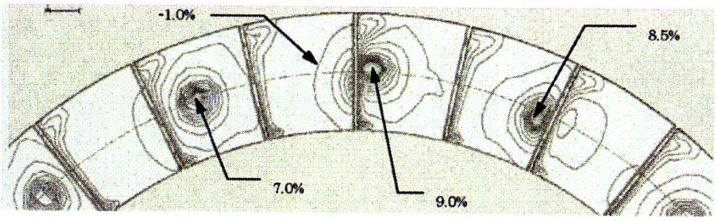

(b) stator T/E

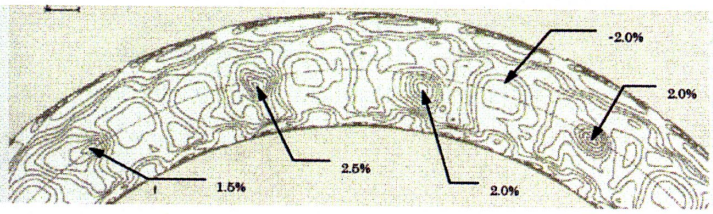

(c) downstream of rotor T/E

Figure 2 Time averaged distribution of total temperature

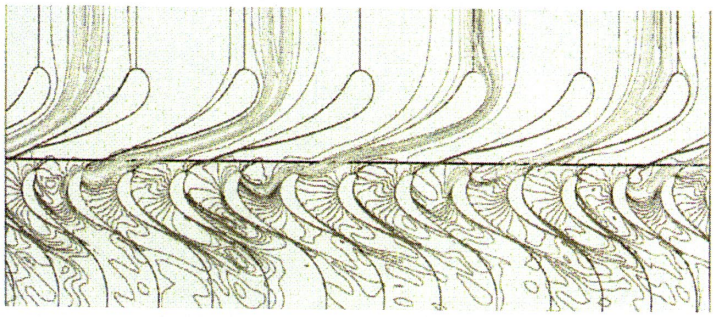

Figure 3 Instantaneous distribution of total temperature (midspan)

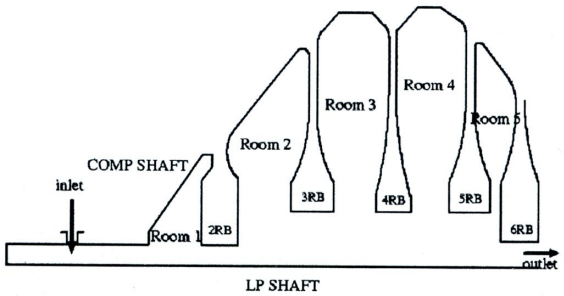

Figure 4 Schematic of high pressure compressor disc cavity

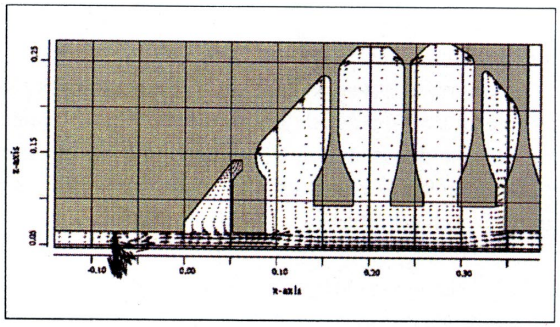

Figure 5 velocity vectors inside HPC disc cavity

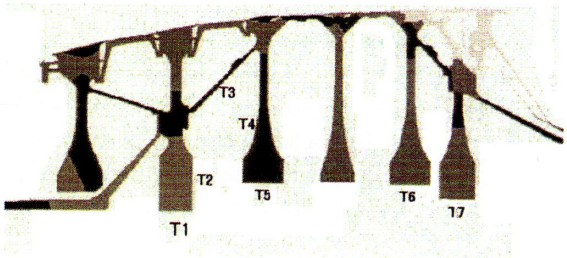

Figure 6 Temperature distribution of HPC disc

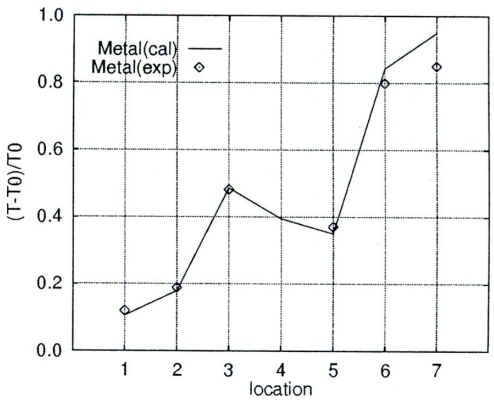

Figure 7 Comparison of distributions of wall temperature

This document is provided by JAXA.

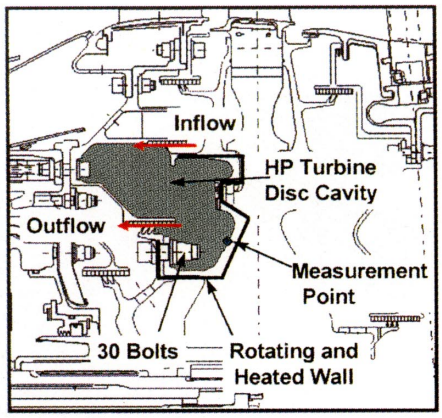

Figure 13 Schematic of high pressure turbine disc cavity

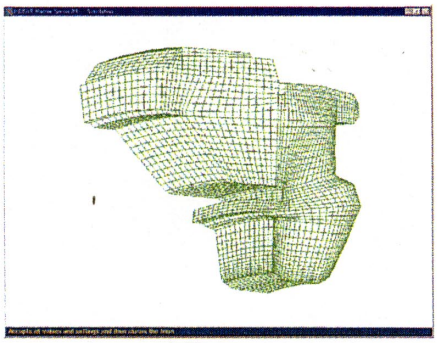

(a) without bolt

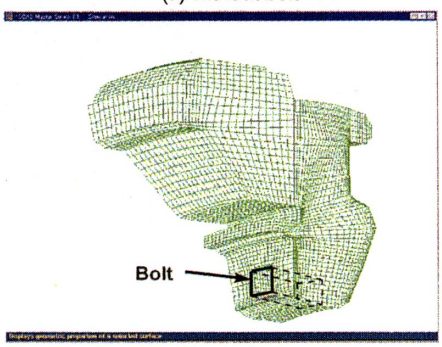

(b) with bolt

Figure 14 Numerical grid of turbine disc cavity

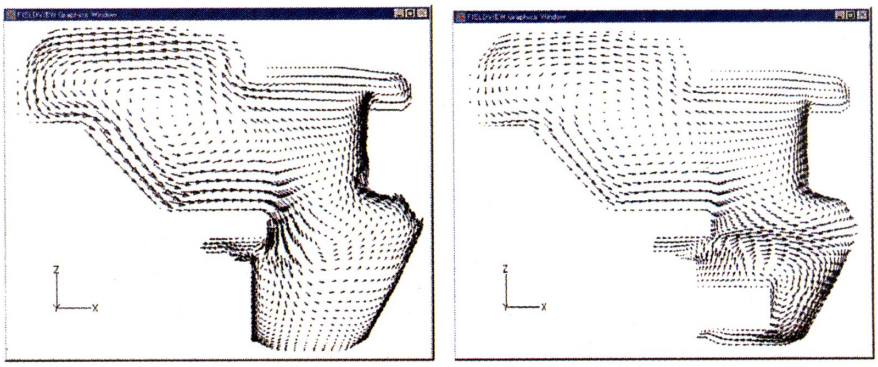

(a) without bolt (b) with bolt

Figure 15 Velocity vectors at center of bolt

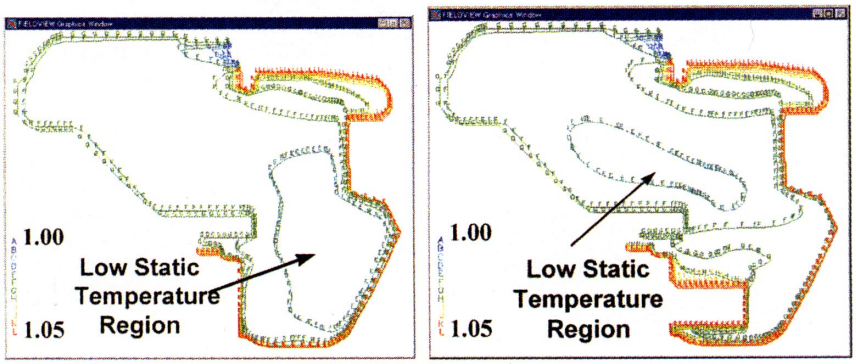

(a) without bolt (b) with bolt

Figure 16 Distributions of normalized temperature at center of bolt

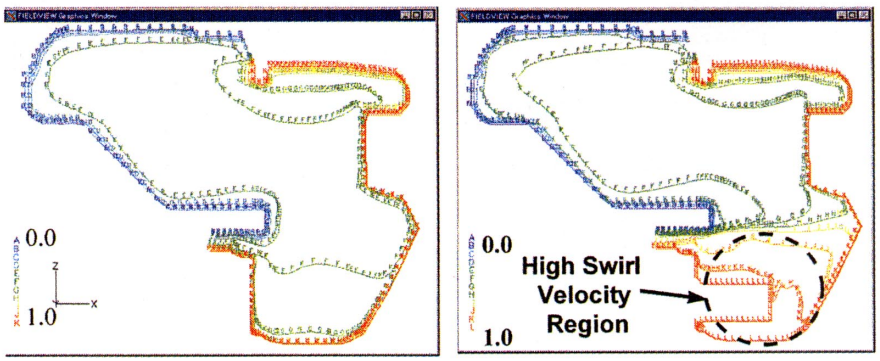

(a) without bolt (b) with bolt

Figure 17 Distributions of swirl ratio at center of bolt

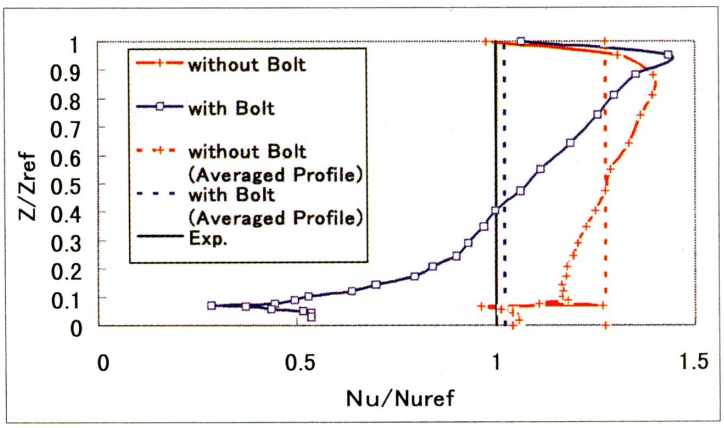

Figure18 Distributions of circumferentially averaged normalized heat transfer ratio at measurement point

This document is provided by JAXA.

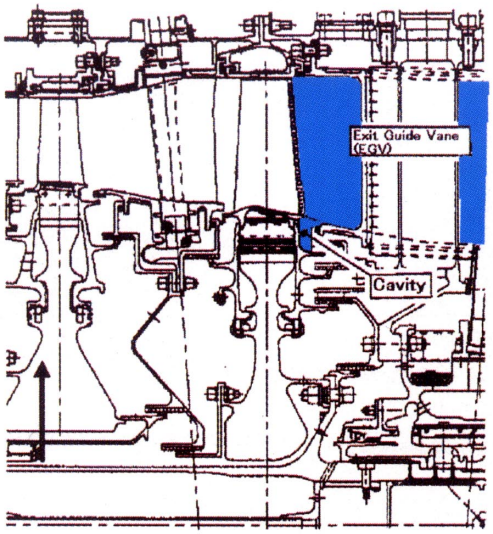

Figure 8 Schematic of EGV and Rim-rear cavity

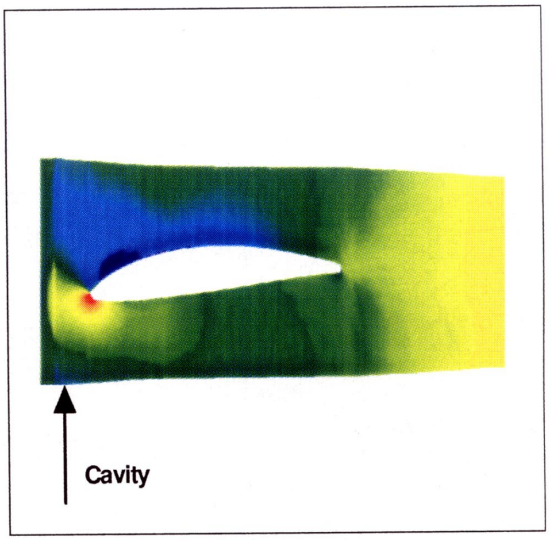

Figure 10 Distribution of static pressure on endwall surface of EGV

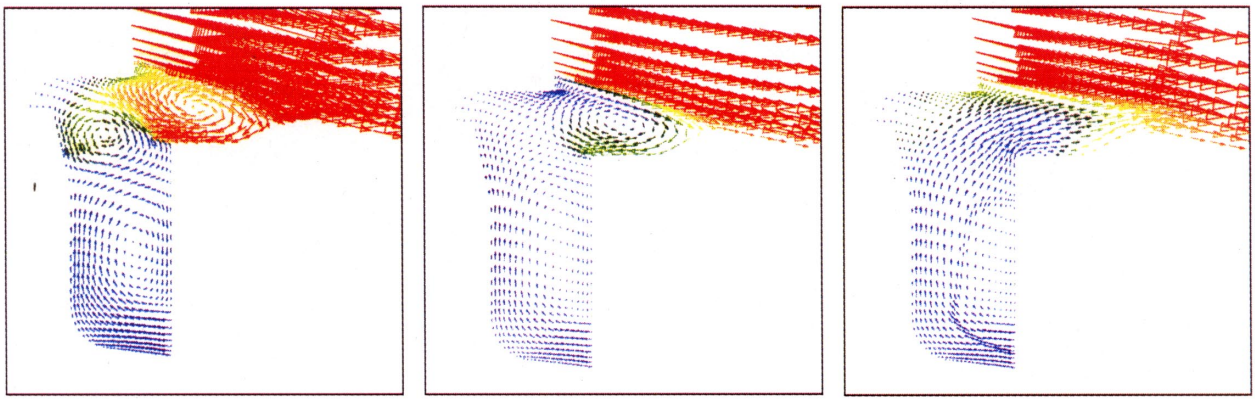

(a) Pos.1 (near EGV L/E) (b) Pos.2 (near EGV pressure surface) (c) Pos. 3 (near EGV suction surface)

Figure 9 Distributions of temperature and velocity vectors inside rim-rear cavity near EGV L/E

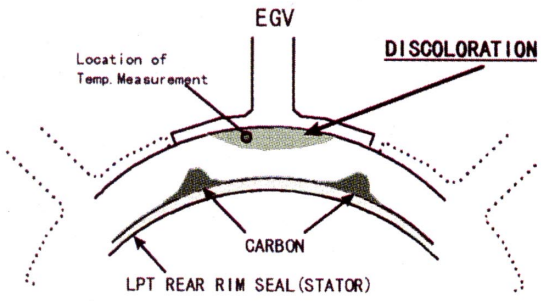

Figure 11 Schematic of discolored region on stator disc surface (Rim-rear cavity)

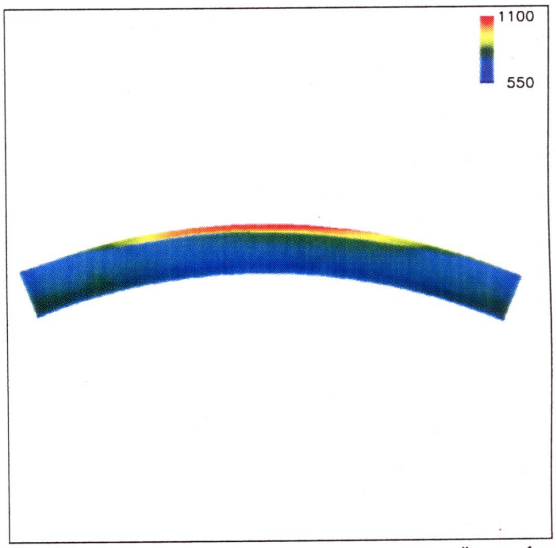

Figure 12 Distribution of temperature on stator disc surface (Rim-rear cavity)

This document is provided by JAXA.